Construction and Building Materials 146 (2017) 755–763

Contents lists available at ScienceDirect

Construction and Building Materials

journal homepage: www.elsevier.com/locate/conbuildmat

Effect of ZnO nanoparticles on thermoelectric properties of cement composite for waste heat harvesting

SeyedAli Ghahari [a], Ehsan Ghafari [a], Na Lu [a,b,*]

[a] Lyles School of Civil Engineering & School of Materials Engineering, Sustainable Materials and Renewable Technology (SMART) Lab, Purdue University, West Lafayette, IN, USA
[b] Birck Nanotechnology Center, Purdue University, West Lafayette, IN, USA

HIGHLIGHTS

- ZnO and AZO nanoparticles resulted in a lower thermal conductivity up to 9%.
- Seebeck coefficient was increased by 17% with increasing the nanoparticles.
- TE properties of cement paste were enhanced after adding ZnO and AZO nanoparticles.
- ZnO and AZO nanoparticles can potentially be used for energy harvesting.

ARTICLE INFO

Article history:
Received 27 January 2017
Received in revised form 14 April 2017
Accepted 18 April 2017
Available online 25 April 2017

Keywords:
Thermoelectric
Renewable energy
Waste heat
Cement composite
Zinc oxide
Aluminum zinc oxide

ABSTRACT

Thermoelectric (TE) technology can directly convert thermal energy into electricity for waste heat harvesting and renewable energy production. However, the potential use of TE technology for energy harvesting in civil infrastructure has not been fully explored yet. In this work, the possibility of developing concrete with TE properties to harvest stored heat in concrete structures have been systematically investigated by incorporating zinc oxides (ZnO) based nanoparticles in cement paste. It was found that the addition of ZnO nanoparticles improved the TE properties of cement paste due to the formation of $Zn(OH)_2$ and increased volume of pore solutions in ZnO-cement composites. The results showed that after adding nanoparticles to the mixture, Seebeck coefficient of cement particles was increased to 17% due to a decrease in the amount of hydration reactions. Thermal conductivity was decreased to 9% due to decreased density and crystallinity of materials, and electrical conductivity was increased to 37% compared to that of plain cement paste because of the increased movement of ions. The apparent thermoelectric properties in ZnO-cement composites indicated its potential use for thermal energy harvesting in concrete structures and pavements.

1. Introduction

Over 60% of energy produced in the U.S. is wasted as heat, which can be directly converted into electrical energy using TE materials through Seebeck effects discovered by Thomas Seebeck [1]. TE technology has been used in military and aerospace applications as a reliable, safe, and durable power source for many space programs to the outer solar systems [2–6]. However, the potential of using TE technology for thermal energy harvesting in civil infrastructures has not been explored, despite a large quantity of waste heat is available including thermal storage in concrete structures, building envelopes, and waste heat in heating, ventilation, and air conditioning (HVAC) systems. For instance, the surface temperature of the concrete infrastructure can increase up to 60 °C in hot climate, while the air temperature remains at 32 °C. This opens up an opportunity for using TE technology to scavenge the wasted thermal energy into electricity. According to a study performed on the US pavement temperature models, the maximum temperature difference between the air temperature and pavement temperature at a depth of 25 mm is 22.5 °C [7]. The average differences between the air temperature and pavement temperature at a depth of 25 mm for different latitudes and air temperature ranges are presented in Table 1. And as it is shown, there is a considerable potential of using TE technology to harvest stored thermal energy for power generation in concrete and concrete asphalt pavement systems.

* Corresponding author at: Lyles School of Civil Engineering & School of Materials Engineering, Sustainable Materials and Renewable Technology (SMART) Lab, Purdue University, West Lafayette, IN, USA.
E-mail address: Luna@purdue.edu (N. Lu).

http://dx.doi.org/10.1016/j.conbuildmat.2017.04.165
0950-0618/

Table 1
Average difference between the air temperature and pavement temperature.

Geographic latitude (°)	Air Temperature (°C)				
	20–25	25–30	30–35	35–40	40–45
<30	–	–	20.2 °C	19.1 °C	–
30–35	–	–	19.8 °C	19.6 °C	–
35–40	14 °C	22.5 °C	18.2 °C	18.7 °C	14.8 °C
40–45	16.5 °C	18.2 °C	17.8 °C	16.4 °C	–
>45	16.9 °C	17.5 °C	14.7 °C	12.1 °C	–

To realize this potential, a new class of concrete with TE properties needs to be developed. Few studies have been performed to investigate the TE properties of cement and concrete materials using silica fume and carbon nanotube. For instance, Wen and Chung [8] studied the Seebeck effect of steel fiber reinforced cement with silica fume incorporation. It was found that adding steel fiber and silica fume to the mixture resulted in a considerable increase up to 17% in the TE power output. Another study on carbon fiber reinforced concrete performed by Wei et al. showed that carbon fibers could enhance the Seebeck effect of concrete to harvest urban outdoor heat during the summer season [8,9]. However, these materials are not applicable for large-scale applications due to their high materials and processing cost. In contrast, ZnO nanoparticle have shown favorable TE properties, low cost, and earth abundance for large-scale application potentials. Additionally, Zinc can be obtained from waste materials, such as Electric arc furnace dust (EAFD), which contain up to 90% zinc for the production of zinc oxide nanoparticles [10]. Coupled with its large bandgap and high exciton binding energy, ZnO nanoparticles have shown remarkable performance in a wide variety of applications, including photocatalytic and photoluminescence, self-cleaning and pollution remediation for structures and environment [11–14], UV-blocking [15–17], and gas sensors [18]. Therefore, there is a rapid growing interest in using nanoparticles in cement pastes to tailor materials' properties [19–25].

To the best of our knowledge, no studies have investigated the feasibility of using ZnO based nanoparticles to enhance the TE properties of cement composites, although ZnO has proven to be an effective TE material [26–28]. To fill this knowledge gap, this study aims to investigate the effect of ZnO and Al doped ZnO (AZO) nanoparticles on TE properties of cement composites, including the Seebeck coefficient, thermal conductivity, and electrical conductivity. Additionally, structure properties of ZnO cement composites have been investigated using thermogravimetry analysis (TGA), gas pycnometer, and scanning electron microscope (SEM) analysis and calorimetry to unravel the structure-property correlations of ZnO-cement composites.

2. Materials and methods

2.1. Materials

The cement used in this study was Portland cement (PC) type I 42.5R, and its chemical compound is presented in Table 2. Physical properties of ZnO and aluminum doped ZnO (AZO) nanoparticles used in this study are presented in Table 3.

Table 2
Chemical properties of cement.

Chemical Analysis (%)	Cement (C)
SiO_2	20.9
Al_2O_3	4.60
Fe_2O_3	3.15
CaO	62.0
MgO	2.00
SO_2	3.60
K_2O	<1
Na_2O	<1
Specific gravity	3.14

To maintain workability, a polycarboxylate ether based superplasticizer (SP) with a density of 1.108 g/cm^3 was used. Water to binder ratio was kept constant at 0.35, five different dosages of ZnO and AZO were added to the mixtures as cement replacement by 0.2, 0.4, 0.6, 0.8, and 1 of weight fractions (wt%) of cement. The total content of the powder including cement and nanoparticles was kept constant in volume. All specimens were cast with a Twister Evolution vacuum mixer, and cured with potable water according to ASTM C150 [29]. Table 4 represents the mixture proportion of all specimens cast in this study.

Electrical conductivity measurement was conducted using cylindrical specimens with the diameter of 70 mm and 35 mm. The electrical conductivity mold set up included two 2.5 mm diameter rods longitudinally placed 20 mm apart from each other. The impedance of the specimens were captured, over a frequency range from 1 MHz to 1 Hz and a 100 mV AC signal, using a Solatron 1260 Impedance Gain-Phase analyzer. The electrical conductivity can be obtained according to the following equation:

$$\sigma = \frac{k}{R} \tag{1}$$

where σ is conductivity (S/m), k is geometry factor (1/m), i.e. 22.15/m^{-1} in this study, and R is bulk resistance (ohm.). The detailed testing method is described elsewhere [30,31], and the geometry factor has been determined according to a commonly accepted method as described in the literature [32–34].

In order to measure the Seebeck coefficient, two surfaces of cement composite cubes (40 × 40 mm^2) were polished with sandpaper. One side was kept at room temperature (23 ± 2 °C) and the other side was placed on a platelet resistance heater (the heat was applied with a rate of 0.01 °C s^{-1} and from the room temperature to 85 °C). Both sides were covered with 5 mm thick copper foils to maintain the thermal contact between the specimen and the heater. Seebeck coefficient was obtained using our homemade apparatus, as shown in Fig. 1. It contains two K-type thermocouples and two copper wires attached to both ends (to the copper plates) of the sample. The temperatures at both sides of samples (T_{hot} and T_{room}) were recorded by Omega Temperature controller (CN616) and voltages (V_{hot} and V_{room}) were recorded by a Kiethly multi-meter Instrument (2182a). CN616 was chosen due to the reason that it connects and response quickly to Kiethly multi-meter Instrument. All the values were captured via a data acquisition (DAQ) card and national instrument (NI) LabView®2015 program, specifically coded for this study by the authors. The LabView surface developed for this specific research is presented in Fig. 2. The temperature of the specimen was increased from 25 °C to 85 °C with the heating rate of 5 °C/min. At each increment, the temperature was held constant for 5 minutes in order to achieve stability in the voltage values. The apparent Seebeck coefficient was then obtained by calculating ΔV/ΔT for each specimen.

Thermal conductivity was measured by a longitudinal guarded comparative calorimeter (LGCC) made according to ASTM E1225-09 [35] and ASTM D5479-12 [36]. Cylindrical samples with dimension of 25.4 mm in diameter and 50.8 mm in height were cast on the date of each experiment, the specimens were then put in a special isolated cylinder (equipped with thermocouples shown in Fig. 3) to ensure one-dimensional heat flow generated by a cold plate. Thermal insulation was applied to reach the steady-state thermal condition for measuring the heat flow of a material. Herein, two Pyrocerams samples with known thermal properties were used as reference samples to measure the heat flow of specimen. The thermal conductivity of the reference sample was obtained according to the following equation [37]:

$$\lambda_{TC} = -0.0061(T) + 4.2013 \tag{2}$$

where λ_{TC} is the thermal conductivity of the Pyroceram (W/mK), and T is the specimen temperature (°C). ThermaCool TC3008 was used as thermal pad. The thickness of the pads was 3 mm and the thermal conductivity was estimated at 3.0 W/m K. The temperatures were monitored with 7 P-type thermocouples with an accuracy of +0.2 °C. The heat was provided via a two-stage cold plate (Cascade CCP-22).

Density measurement were performed with AccuPycII 1340 nitrogen gas pycnometer according to ASTM D5550 [38]. Thermal gravimetric analysis (TGA) was performed with TGA Quantachrome Q50. Thermogravimetric analysis (TGA) was conducted to determine the portlandite (CH) content and the amount of bound water of dried cement paste. The estimation of the degree of hydration (DOH) was obtained by calculating based on the mass loss difference from temperature 380 °C and 460 °C, which is associated with dehydroxylation of the $Ca(OH)_2$ [39].

Table 3
Properties of ZnO nanoparticles.

Formula	Aluminum content	Specific Surface area (m^2/g)	Purity	Crystal Phase	Mean Diameter(nm)	Density (g/cm^3)
ZnO	0	54 ± 20	>99.9 (wt%)	Zincite (hexagonal)	20 ± 5	5.6
AZO	0.2 (wt%)	54 ± 20	>99.9 (wt%)	Zincite (hexagonal)	20 ± 5	5.6

Table 4
Composition of pastes mixture (by weight, g/cm^3).

		Cement	Water	SP	ZnO	Al-ZnO
Ref	PC	593.9	207.9	2.4	0	0
ZnO Mixtures	ZnO_0.2	592.7	207.9	2.4	1.18	0
	ZnO_0.4	591.5	207.9	2.4	2.37	0
	ZnO_0.6	590.3	207.9	2.4	3.56	0
	ZnO_0.8	589.1	207.9	2.4	4.75	0
	ZnO_1	587.9	207.9	2.4	5.93	0
Al-ZnO Mixtures	AZO_0.2	592.7	207.9	2.4	0	1.18
	AZO_0.4	591.5	207.9	2.4	0	2.37
	AZO_0.6	590.3	207.9	2.4	0	3.56
	AZO_0.8	589.1	207.9	2.4	0	4.75
	AZO_1	587.9	207.9	2.4	0	5.93

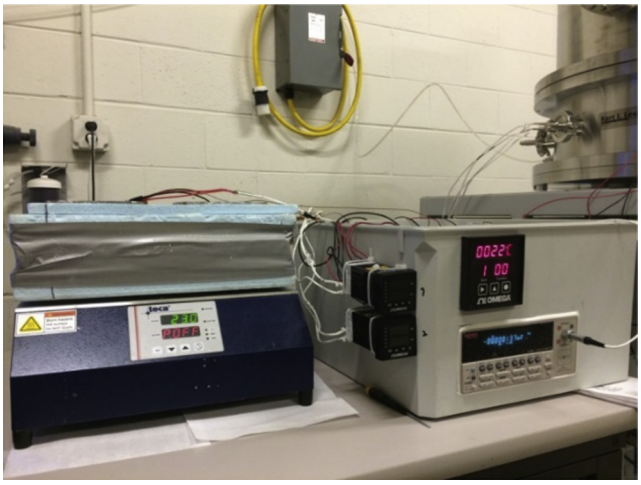

Fig. 1. Seebeck coefficient test set up.

Field emission-scanning electron microscope (FE-SEM) using FEI Quanta 3D FEG and energy-dispersive X-ray spectroscopy (EDX) were also performed in order to study the microstructure and chemical composition of the cement paste samples.

3. Results and discussion

3.1. Electrical conductivity

The effect of different weight fractions of ZnO and AZO nanoparticles on the electrical conductivity of the specimens at the ages of 14, 28, and 90 days is illustrated in Fig. 4. As shown, in general, the electrical conductivity decreases with time. This can be explained by the following equation which considers only the fluid phase to be conductive [40],

$$\sigma = \sigma_0 \varphi_0 \beta_0 \tag{3}$$

where σ_0 is conductivity of the pore solution (S/m), φ_0 is volume fraction of pores, and β_0 is connectivity of pore structure. This happens because the conductive pore fluid reduces with time and the conduction path becomes more tortuous accordingly [41–43]. Moreover, in micro-scale, the electrical conductivity is related to the mobility of electrons and holes. The electrical conductivity for a p-type semiconductor is calculated according to the following equation:

$$\sigma = ne\mu_h \tag{4}$$

where σ is conductivity of the materials (S/m), n is the concentration of holes (m^{-3}), e is the elementary charge (C), and μ_h is the hole mobility ($m^2/V.s$). In this study, the addition of ZnO nanoparticles acted as p-type carriers, which increased hole concentrations in ZnO-cement composites.

According to Fig. 4, the electrical conductivity increases with increasing the amount of nanoparticles. As presented in Fig. 4, at the age of 90 days, when almost the hydration reactions have been completed, the conductivity of AZO_0.4 is measured as 27.2×10^{-3} S/m which is 37% more than that of the plain cement paste. However, the values for the samples that have more than 0.6% wt cement ZnO and AZO nanoparticle are significantly higher than that of the reference sample. The previous studies show that the addition of 0.6% wt ZnO nanoparticle or more results in a significant delay in hydration process of cement [44]. When ZnO reacts with water, zinc hydroxide is produced. This will be attached to the circumference of C-S-H layers which causes a significant retardation effect [45,46]. It is well known that when Zn $(OH)_2$ reacts with calcium ions and transform into crystalline $CaZn_2(OH)_6{\cdot}2H_2O$, according to the following equation. This would cause a significant destruction on the impermeable layer [47].

$$Zn(OH)_4^{2-} + Ca^{++} + H_2O \rightarrow Ca(Zn(OH)_3)_2 \cdot 2H_2O + 2OH^- \tag{5}$$

The amorphous layer of $Zn(OH)_2$ is the main cause of prohibiting the C_3S phase participation in hydration process [48]. Therefore, the formation of less hydration products may lead to an increase in the volume fraction and connectivity of pore structure which directly influence the electrical conductivity of the cement paste (Eq. (2)).

The results indicated that the cement paste containing AZO exhibits lower electrical conductivity compare to cement paste with ZnO nanoparticles. When AZO nanoparticles were mixed with cement particles, the cement particles would be covered by aluminum that could cause the acceleration of the hydration process and produce more hydration products. The latter will reduce the volume fraction and connectivity of pore structures which consequentially reduce the electrical conductivity.

Thermogravimetry analysis of DOH was performed in order to prove the discussion above. The analysis indicated that ZnO nanoparticles can prohibit the hydration process at early ages,

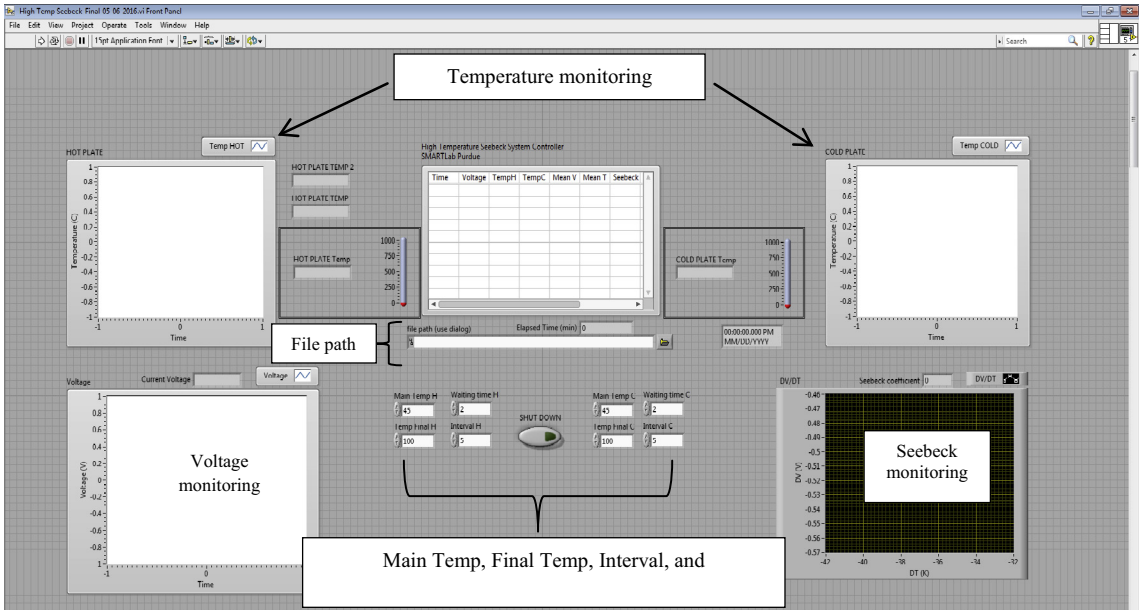

Fig. 2. Lab View program for temperature controlling.

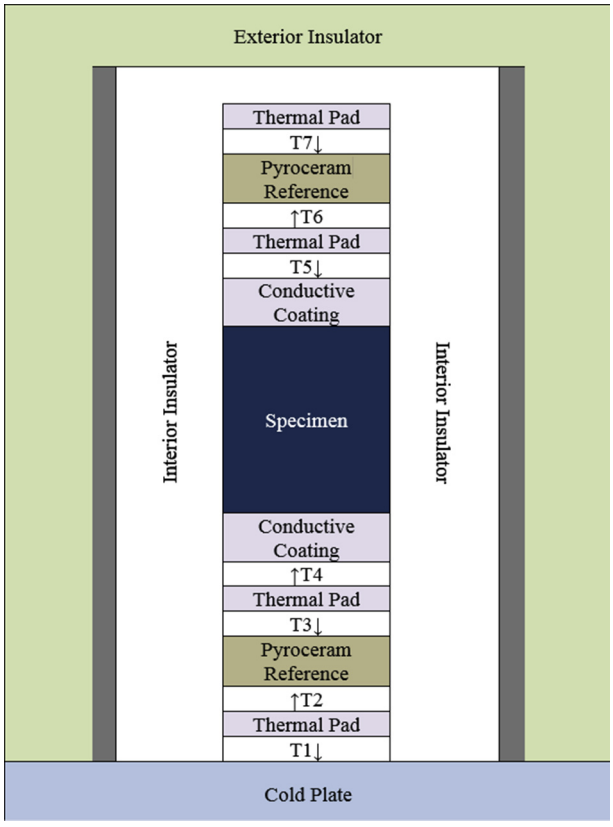

Fig. 3. LGCC device schematic set up.

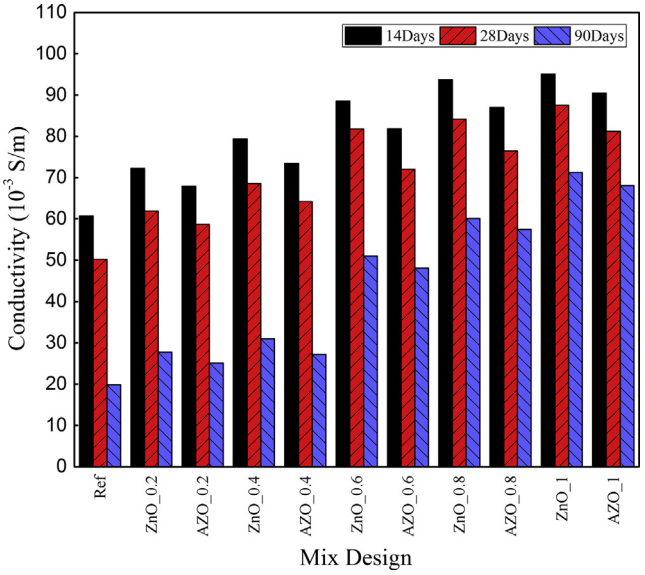

Fig. 4. Electrical conductivity vs. ZnO (wt%) and AZO (wt%) at the age of 14, 28, and 90 days.

especially when added in the amount of more than 0.6% wt amount. Mass loss of water is attributed to the hydration reactions. The mass losses of cement paste for all specimens were obtained by thermal gravimetric analysis and the corresponding DOH is presented in Fig. 5. According to the results, the mass loss (%) of the PC was increased 30% with the age. ZnO-cement mixes showed a decrease in the amount of the mass loss. High amount of ZnO nanoparticles increased the overall mass loss from 9.83% to 11.65%. The value for AZO samples was calculated 14%–17% higher than that of the ZnO samples. This can be attributed to the nucleation and growth poisoning of C-S-H caused by ZnO nanoparticles [49]. The DOH for PC was increased 5% with age. Both ZnO and AZO mixes showed a decrease in the amount of DOH while increasing the concentration of nanoparticles. A substantial difference of DOH in reference samples and nanoparticle- cements was observed at the age of 3 and 7 days. However, at the age of 28 days, AZO_0.2 and AZO_0.4 showed a slight decrease in the amount of DOH compared with PC, i.e. 6% and 10% lower than that of the PC mix, respectively.

3.2. Seebeck coefficient

The results of apparent Seebeck coefficients for selected specimens are illustrated in Fig. 6. The test was performed three times

in order to achieve better accuracy and less overall error. It can be observed that the Seebeck coefficient increases with increasing the nanoparticles content until it reaches to the value of 0.4% wt cement AZO nanoparticles. The Seebeck coefficient results obtained at the age of 28 days are presented in Table 5. The results indicate that the Seebeck coefficient is 0.188 μV/K at room temperature for the samples with 0.4 wt% AZO nanoparticles. The Seebeck coefficient for the reference specimen with no added nanoparticle is measured as 0.161 μV/K, therefore, a 17% increase in the Seebeck coefficient in AZO_0.4 sample is observed. Seebeck coefficient is an indication of the average energy of electron in each material, and positive value of Seebeck is attributed to p-type behavior of the specimen. This finding is in consistent with existing literatures in that the hole conduction is a predominant factor to enhance the Seebeck coefficient in cementitious materials [8].

The increase in the Seebeck coefficient of the cement paste with ZnO and AZO nanoparticles may also be related to a decrease in the amount of hydration reactions. The results are in agreement with the electrical conductivity analysis discussed above. The results indicated that the Seebeck values for the samples containing more than 0.6% wt were lower than that of ZnO_0.4 and AZO_0.4 which proves the fact that adding more than 0.4% wt nanoparticles in cement would not enhance the Seebeck effect of cement composites. Fig. 7 shows the SEM image of microstructure of cement composites with ZnO_0.4 and AZO_0.4 at the age of 28 days. The results of energy-dispersive X-ray spectroscopy (EDX) are presented under each micrograph. As shown in Fig. 7(a) and the corresponding EDX associated with K-α peaks, the cement particle is partially covered with ZnO and no significant hydration product is observed. For the specimen with ZnO_0.4, the EDX analysis showed that the amount of silicate (Si) and calcium (Ca) for the cement particle covered with ZnO is about 20% lower than that of the uncovered spot, which indicates that hydration is not completely occurred.

In contrast, Fig. 7(b) shows the hydration products were formed around the cement particle with AZO nanoparticle incorporations. When hydration occurs in the presence of cement and water, C-S-H gel is formed. Higher amount of Ca and Si observed around cement particles could be attributed to the higher amount of hydration. AZO_0.4 EDX analysis showed that the amount of Si, Ca, and Al around the spot that has covered the cement particle is higher than that of the uncovered cement particle. Additionally, silicate (Si), Calcium (Ca), and Aluminum (Al) weight percent for AZO_0.4 cement composites is considerably higher than that of the cement particle incorporated with ZnO nanoparticles. It is important to note that the presented EDX result is obtained from the fractured surface of the specimens and is associated with the secondary mode. Nevertheless, our SEM and EDX results of ZnO and AZO were in consistent with other results of the ZnO and AZO on hydration of mixture.

Moreover, AZO nanoparticles have a significant higher surface area to volume ratio compared to that of common concrete particles, therefore they work as filler to form a better interfacial transition zone (ITZ) and a denser microstructure of cement composites when added in mixtures. Previous literature has discussed that Al dopants fill Zn vacancies in an AZO molecule. Zn components are covered with metallic part with Al defects, and electrons can be transported from one Zn packet to another. An Al site coordinated to six oxygen atoms and four and five fold coordinated aluminum sites surround ZnO nanoparticles in AZO [50]. Therefore, when AZO nanoparticles are mixed with cement particles, the cement particles will be covered by aluminum that can cause the acceleration of the hydration process. On the other hand, ZnO nanoparticles cause the reduction in the hydration rate. Therefore, adding aluminum to zinc oxide can improve the hydration process and the DOH, which can enhance the electrical conductivity of the matrix with AZO due to an increase in the ionic strength of the pore solution as our experimental results indicated.

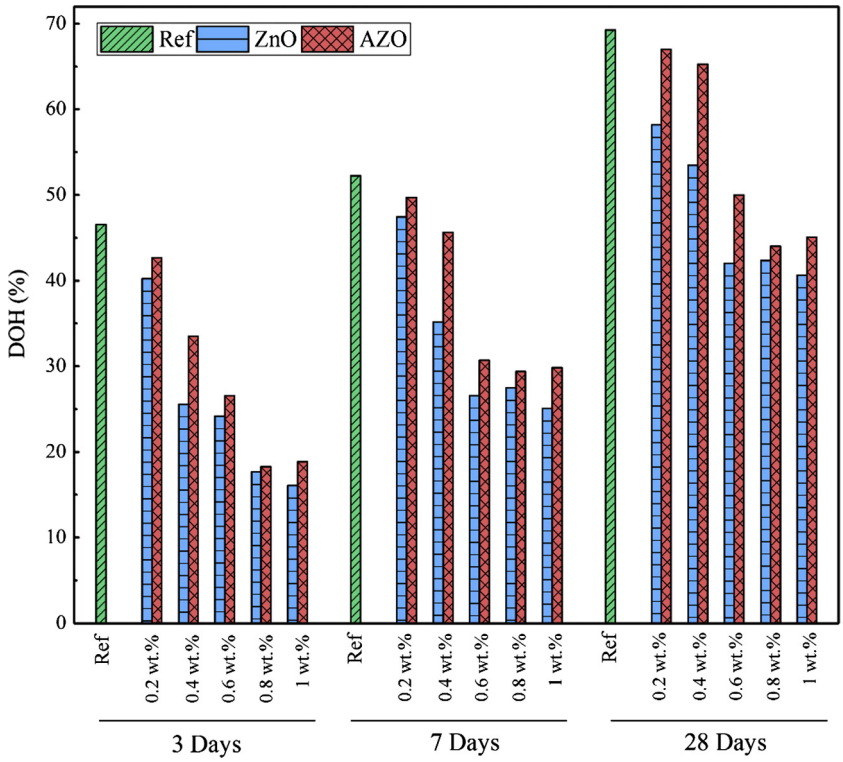

Fig. 5. Degree of hydration for all specimens.

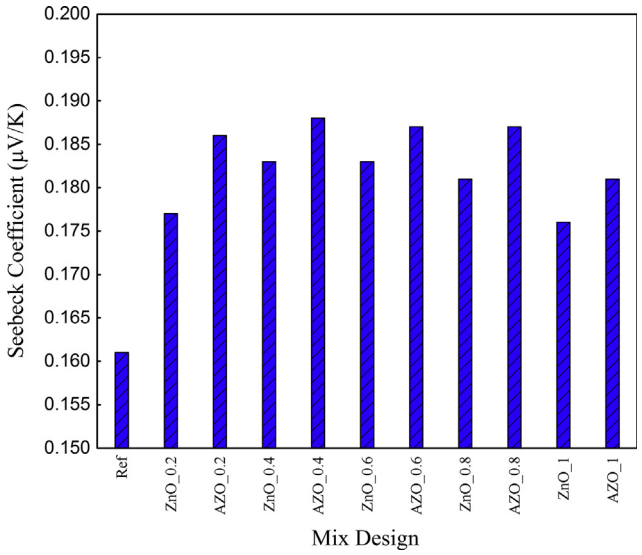

Fig. 6. Seebeck coefficient calculated at the age of 28 days.

3.3. Thermal conductivity

The thermal conductivity (λ) of the specimens was calculated according to the following equation [51,52]:

$$\lambda = \frac{L \times (q_B + q_T)}{T_T - T_B} \quad (6)$$

where q_B is the average heat flow of the bottom per unit area (W/m^2) through mortar sample, q_T is the average heat flow of the top per unit area (W/m^2) through mortar sample, T_T is the average temperature of the top (K), T_B is the average temperature of the bottom (K) and L is length of the sample (m).

The density and thermal conductivity of the samples at the age of 28 days are presented in Fig. 8. As shown, the addition of ZnO and AZO nanoparticles to the cement mixture leads to a comparatively lower density. The previous study by authors confirmed that the addition of both ZnO and AZO resulted in a considerable increase in viscosity. The water demand of cement paste increases due to the higher specific surface area of the nanoparticles. Thus, nanoparticles absorb a significant amount of the available water in the mix, which results in a considerable decrease in workability.

Table 5
Seebeck coefficient test results at the age of 28 days.

Reading Temp. (K)	Samples										
	Ref	ZnO 0.2	AZO 0.2	ZnO 0.4	AZO 0.4	ZnO 0.6	AZO 0.6	ZnO 0.8	AZO 0.8	ZnO 1	AZO 1
313.15	2.385	2.345	2.442	2.523	2.665	2.392	2.858	2.368	2.829	2.321	2.773
328.15	5.396	5.851	6.512	5.472	6.684	6.085	6.923	5.963	6.784	5.784	6.581
343.15	7.805	8.615	8.949	8.101	9.224	8.701	9.610	8.440	9.514	8.102	9.228
358.15	9.653	10.304	10.977	10.818	11.224	10.716	11.264	10.609	11.292	10.396	10.953
Seebeck Coeff. (μV/K)	0.161	0.177	0.186	0.183	0.188	0.183	0.187	0.181	0.187	0.176	0.181

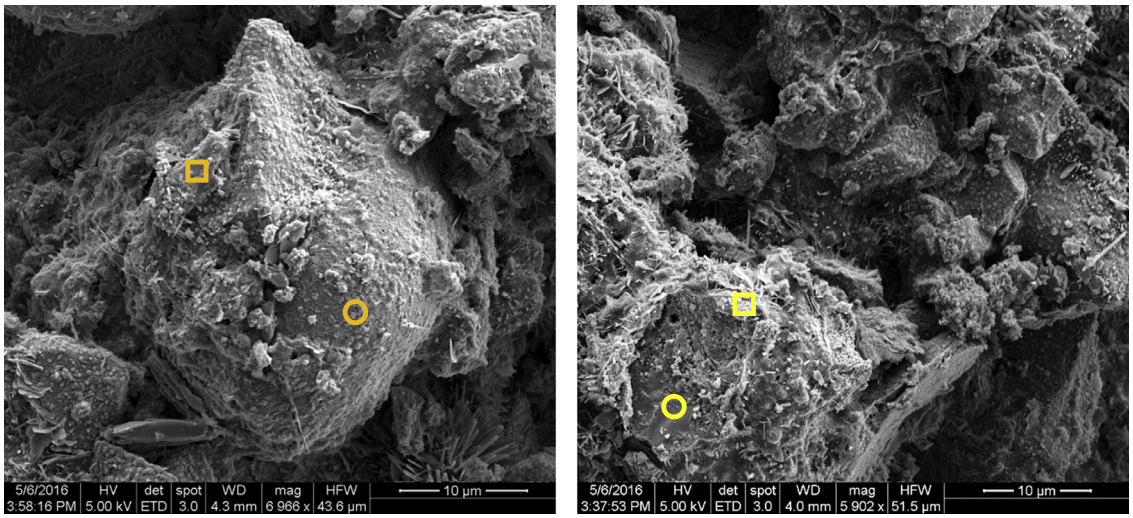

Cement particle covered with (a) ZnO_0.4							Cement particle covered with (b) AZO_0.4					
EDX Results: Elements (Weight %)												
	O	Si	Ca	Fe	Zn	Al	O	Si	Ca	Fe	Zn	Al
□	36.87	7.91	40.12	7.24	2.61	5.25	28.19	11.20	43.28	9.89	0.2	7.24
○	33.2	9.92	44.15	8.62	0.10	4.01	34.51	9.64	41.36	9.49	0.1	4.91

Fig. 7. Cement particle covered with (a) ZnO0.4 and (b) AZO0.4 at 28 days.

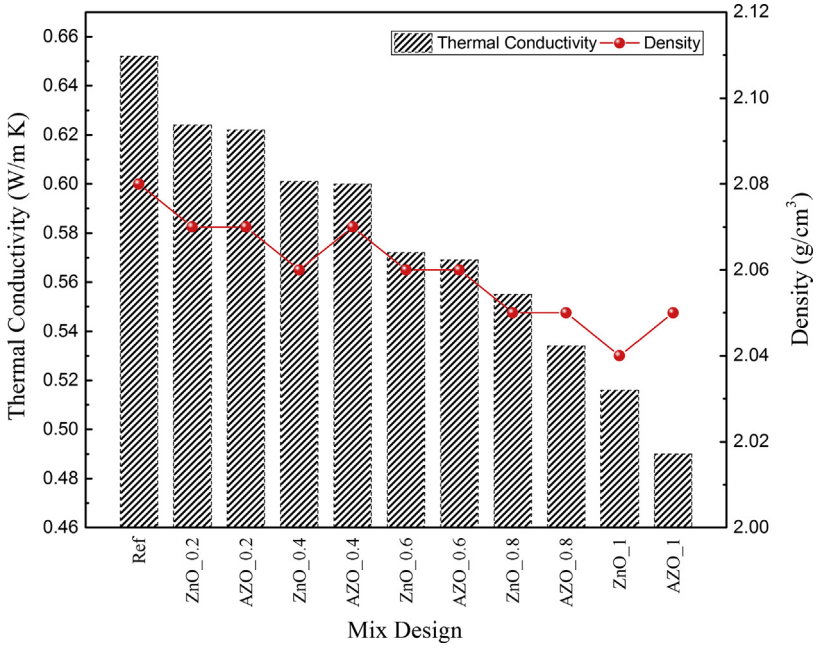

Fig. 8. Thermal conductivity of the samples at the age of 28 days.

Table 6
Thermoelectric properties of the specimen at the age of 28 days.

	Samples										
	Ref	ZnO 0.2	AZO 0.2	ZnO 0.4	AZO 0.4	ZnO 0.6	AZO 0.6	ZnO 0.8	AZO 0.8	ZnO 1	AZO 1
Seebeck Coeff. (μV/K)	0.161	0.177	0.186	0.183	0.188	0.183	0.187	0.181	0.187	0.176	0.181
Thermal Conduct. (W/mK)	0.652	0.624	0.622	0.601	0.6	0.572	0.569	0.555	0.534	0.516	0.49
Electrical Conduct. 10^{-3} (S/m)	50.21	61.87	58.67	68.56	64.22	81.78	72.03	84.14	76.42	87.55	81.23

As a consequence, there was no sufficient water available for allowing particles free movement so that the higher shear stress was required to breakdown the cement paste structures, which resulted in a higher viscosity [53,54]. Also, the previous study showed that, the ZnO, AZO and cement particles compete to adsorb SP which does not leave enough admixture available for adsorption by cement particles to be efficiently dispersed, which also leads to an increase in viscosity [55]. As such, AZO- cement exhibited higher viscosity resulted in a stiffer mix compare to pastes containing ZnO. This properties can be attributed to higher adsorption isotherm of AZO compare to ZnO [55]. Higher viscosity of the sample containing nanoparticles shows an increase in the amount of entrapped air in the mixture, which finally results in a lower density. It has been well reported that the thermal conductivity has direct relation with the concrete density [56–60].

Although the general trend of our experimental data is consistent with the existing literature, we have also observed that crystallinity may play a role in affecting thermal conductivity of nanoparticle-cement mixture. It has been reported that thermal conductivity of crystalline structure is about 15 times higher than its amorphous counterpart [57], so that the concretes with amorphous structure tends to have lower thermal conductivity [61,62]. During the cement hydration, $Zn(OH)_2$ amorphous layer is formed which covers clinker particles [48]. The following reaction shows the formation of $Zn(OH)_2$:

$$Zn^{2+} + 2OH^- -> Zn(OH)_2 \quad (7)$$

In fact, the higher amount of ZnO and AZO nanoparticles cause the microstructure of the cement paste becomes more amorphous leading to a lower thermal conductivity. Therefore, $Zn(OH)_2$ amorphous layer also affects the thermal conductivity of the cement paste incorporated with nanoparticles. Given the fact that Seebeck coefficient is the dominant factor among all three TE related material properties due to the square effect, cement composites with AZO_0.4 nanoparticles is found to give the best results in terms of the thermoelectric properties, as presented in Table 6.

4. Conclusion

In this paper, the effects of ZnO and AZO nanoparticles on TE properties and structural properties of cement mixtures was investigated. The results indicated that the Seebeck coefficient was increased by 17% with increasing the nanoparticles. The increase in the Seebeck coefficient of the cement paste with ZnO and AZO nanoparticles may be related to a decrease in the amount of hydration reactions. It was found that the addition of ZnO and AZO nanoparticles results in a lower thermal conductivity up to 9%. The results indicated that the density along with the amorphous structure has a direct effect on the thermal conductivity of the cement paste. The results showed that the addition of ZnO and AZO resulted in an increase in electrical conductivity up to 37%. This might be due to the retardation effect of ZnO nanoparticles on hydration process of cement paste. Therefore, the formation of less hydration products may lead to an increase in the volume fraction and connectivity of pore structure which increases the electrical conductivity of the cement paste. In summary, the TE properties of cement paste have been enhanced by adding ZnO and AZO nanoparticles. This suggests that the resulting materials can potentially be used for energy harvesting to convert stored thermal energy in concrete infrastructures to electrical power.

Acknowledgments

The authors are grateful to Prof. Jason Weiss at Oregon State University and Dr. Yaghoob Farnam at Drexel University for providing the LGCC device, and Prof. Jan Olek at Purdue University for valuable discussions.

References

[1] Z. Chen, G. Han, L. Yang, L. Cheng, J. Zou, Nanostructured thermoelectric materials: current research and future challenge, Prog. Nat. Sci. Mater. Int. 22 (6) (2012) 15.
[2] A. Sanchez-Torres, Radioisotope Power Systems for Space Applications, in: P.N. Singh (Ed.), InTech, 2011.
[3] R. Furlong, E. Wanhlquist, U.S. Space, Missions using radioisotope power systems, Nuclear News 42 (4) (1999) 26–34.
[4] G. Bennett, Space nuclear power: opening final frontier, in: 4th International Energy Conversion Engineering Conference and Exhibit (IECEC). 2006: San Diego, California.
[5] E.K. Lee et al., Large thermoelectric figure-of-merits from SiGe nanowires by simultaneously measuring electrical and thermal transport properties, Nano Lett. 12 (6) (2012) 2918–2923.
[6] F. Pacheco-Torgal, S. Jalali, Nanotechnology: advantages and drawbacks in the field of construction and building materials, Constr. Build. Mater. 25 (2) (2011) 582–590.
[7] A. Mohseni, LTPP seasonal asphalt concrete (AC) pavement temperature models. 1998, FHWA-RD-97-103. p. 1–71.
[8] S. Wen, D.D.L. Chung, Enhancing the Seebeck effect in carbon fiber-reinforced cement by using intercalated carbon fibers, Cem. Concr. Res. 30 (8) (2000) 1295–1298.
[9] J. Wei et al., Energy harvesting from solar irradiation in cities using the thermoelectric behavior of carbon fiber reinforced cement composites, RSC Adv. 4 (89) (2014) 48128–48134.
[10] R.Z. Al-Zaid, F.H. Al-Sugair, A.I. Al-Negheimish, Investigation of potential uses of electric-arc furnace dust (EAFD) in concrete, Cem. Concr. Res. 27 (2) (1997) 267–278.
[11] G. Kenanakis, D. Vernardou, N. Katsarakis, Light-induced self-cleaning properties of ZnO nanowires grown at low temperatures, Appl. Catal. A 411–412 (2012) 7–14.
[12] S.A. Khayyat et al., Synthesis and characterizations of Cd-doped ZnO multipods for environmental remediation application, J. Nanosci. Nanotechnol. 12 (11) (2012) 8453–8458.
[13] Q. Li et al., Self-cleaning performance of TiO2-coating cement materials prepared based on solidification/stabilization of electrolytic manganese residue, Constr. Build. Mater. 106 (2016) 236–242.
[14] A.A. Essawy, S.A.E. Aleem, Physico-mechanical properties, potent adsorptive and photocatalytic efficacies of sulfate resisting cement blends containing micro silica and nano-TiO 2, Constr. Build. Mater. 52 (2014) 1–8.
[15] N.J. Lowe, Sunscreens: Development: Evaluation, and Regulatory Aspects, CRC Press, 1996.
[16] D.B. Brown et al., Common fluorescent sunlamps are an inappropriate substitute for sunlight, Photochem. Photobiol. 72 (3) (2000) 340–344.
[17] S. Bogutyn et al., Rejuvenation techniques for mortar containing photocatalytic TiO2 material, Constr. Build. Mater. 96 (2015) 96–101.
[18] A.A. Tomchenko et al., Semiconducting metal oxide sensor array for the selective detection of combustion gases, Sens. Actuators B Chem. 93 (1) (2003) 126–134.
[19] E. Jeoffroy et al., Iron oxide nanoparticles for magnetically-triggered healing of bituminous materials, Constr. Build. Mater. 112 (2016) 497–505.
[20] S. Sharma, N.C. Kothiyal, Facile growth of carbon nanotubes coated with carbon nanoparticles: a potential low-cost hybrid nanoadditive for improved mechanical, electrical, microstructural and crystalline properties of cement mortar matrix, Constr. Build. Mater. 123 (2016) 829–846.
[21] M. Heikal, S.A. El Aleem, W. Morsi, Characteristics of blended cements containing nano-silica, HBRC J. 9 (3) (2013) 243–255.
[22] Saleh Abd El-Aleem, A.E.R. Ragab, Chemical and physico-mechanical properties of composite cements containing micro- and nano-silica, Int. J. Civ. Eng. Technol. (IJCIET) 6 (5) (2015) 45–64.
[23] S.A.E. Aleem, M. Heikal, W. Morsi, Hydration characteristic, thermal expansion and microstructure of cement containing nano-silica, Constr. Build. Mater. 59 (2014) 151–160.
[24] E. Ghafari, H. Costa, E Júlio, Critical review on eco-efficient ultra high performance concrete enhanced with nano-materials, Constr. Build. Mater. 101 (Part 1) (2015) 201–208.
[25] E. Ghafari, M. Arezoumandi, H. Costa, E. Júlio, Influence of nano-silica addition on durability of UHPC, Constr. Build. Mater. 94 (2015) 181–188.
[26] K.P. Ong, David J. Singh, Ping Wu, Analysis of the thermoelectric properties of n-type ZnO, Physical Review B 83 (11) (2011) 115110.
[27] P. Jood, Rutvik J. Mehta, Yanliang Zhang, Germanas Peleckis, Xiaolin Wang, Richard W. Siegel, Theo Borca-Tasciuc, Shi Xue Dou, Ganpati Ramanath, Al-doped zinc oxide nanocomposites with enhanced thermoelectric properties, Nano Lett. 11 (10) (2011) 4337–4342.
[28] M. Ohtaki, Kazuhiko Araki, Kiyoshi Yamamoto, High thermoelectric performance of dually doped ZnO ceramics, J. Electron. Mater. 38 (7) (2009) 1234–1238.
[29] ASTMC150, American Society for Testing and Materials, ASTM C-150 Standard specification for Portland cement, 2012.
[30] M.R. Nokken, R.D. Hooton, Electrical conductivity testing, Concr. Int. 28 (10) (2006) 58–63.
[31] F. Rajabipour, J. Weiss, Electrical conductivity of drying cement paste, Mater. Struct. 40 (10) (2007) 1143–1160.
[32] J. Castro, R. Spragg, J. Weiss, Water absorption and electrical conductivity for internally cured mortars with a W/C between 0.30 and 0.45, J. Mater. Civ. Eng. 24 (2) (2011) 223–231.
[33] A. Peled et al., Electrical impedance spectra to monitor damage during tensile loading of cement composites, ACI Mater. J. 98 (4) (2001) 313–322.
[34] W.J. Weiss, Prediction of Early-Age Shrinkage Cracking in Concrete Elements, 1999.
[35] ASTME1225-09, Standard test method for thermal conductivity of solids by means of the guarded-comparative-longitudinal heat flow technique, Annual Book of ASTM Standards, ASTM International, West Conshohocken, PA, 2009.
[36] ASTMD5470-12, Standard Test Method for Thermal Transmission Properties of Thermally Conductive Electrical Insulation Materials, Annual Book of ASTM Standards, ASTM International, West Conshohocken, PA, 2012.
[37] Y. Farnam et al., Measuring freeze and thaw damage in mortars containing deicing salt using a low-temperature longitudinal guarded comparative calorimeter and acoustic emission, Adv. Civ. Eng. Mater. 3 (1) (2014) 23.
[38] ASTMD5550, American society for testing and materials, ASTM D-5550 Standard Test Method for Specific Gravity of Soil Solids by Gas Pycnometer, 2014.
[39] B. El-Jazairi, J. Illston, A simultaneous semi-isothermal method of thermogravimetry and derivative thermogravimetry, and its application to cement pastes, Cem. Concr. Res. 7 (3) (1977) 247–257.
[40] W.J. McCarter, R. Brousseau, The A.C. response of hardened cement paste, Cem. Concr. Res. 20 (6) (1990) 891–900.
[41] A. Ramezanianpour, S. Ghahari, M. Esmaeili, Effect of combined carbonation and chloride ion ingress by an accelerated test method on microscopic and mechanical properties of concrete, Constr. Build. Mater. 58 (2014) 138–146.
[42] S.A. Ghahari et al., An accelerated test method of simultaneous carbonation and chloride ion ingress: durability of silica fume concrete in severe environments, Adv. Mater. Sci. Eng. 2016 (2016) 12.
[43] S. Ghahari, A. Mohammadi, A. Ramezanianpour, Performance assessment of natural pozzolan roller compacted concrete pavements, Case Stud. Constr. Mater. (2017).
[44] T. Nochaiya et al., Microstructure, characterizations, functionality and compressive strength of cement-based materials using zinc oxide nanoparticles as an additive, J. Alloy. Compd. 630 (2015) 1–10.
[45] M. Yousuf et al., The interfacial chemistry of solidification/stabilization of metals in cement and pozzolanic material systems, Waste Manage. 15 (2) (1995) 137–148.
[46] M. Gawlicki, D. Czamarska, Effect of ZnO on the hydration of Portland cement, J. Therm. Anal. 38 (9) (1992) 2157–2161.
[47] M. Gawlicki, D. Czamarska, Effect of ZnO on the hydration of Portland cement, J. Therm. Anal. 38 (9) (1992) 2157–2161.
[48] K. Behfarnia, A. Keivan, The effects of TiO_2 and ZnO nanoparticles on physical and mechanical properties of normal concrete, Asian J. Civ. Eng. 14 (4) (2013) 517–531.
[49] F.F. Ataie et al., Comparison of the retarding mechanisms of zinc oxide and sucrose on cement hydration and interactions with supplementary cementitious materials, Cem. Concr. Res. 72 (2015) 128–136.
[50] Y.S. Avadhut et al., Structural investigation of aluminium doped ZnO nanoparticles by solid-state NMR spectroscopy, Phys. Chem. Chem. Phys. 14 (33) (2012) 11610–11625.
[51] D.A. Anderson, J.C. Tannehill, R.H. Pletcher, Computational Fluid Mechanics and Heat Transfer, Hemisphere Publishing, New York, NY, 1984, p. 599. Medium: X; Size.
[52] F. Kreith, W.Z. Black, R.H. Pletcher, Basic Heat Transfer, Harper and Row, Publishers, Incorporated, New York, NY, 1984, p. 558. Medium: X; Size.
[53] A. Korpa, R. Trettin, Ultra high performance cement-based composites with advanced properties containing nanoscale pozzolans, in Proceedings of the Second International Symposium on Ultra High Performance Concrete, Kassel, Germany, 2008.
[54] E. Ghafari, H. Costa, E. Júlio, A. Portugal, L. Durães, The effect of nanosilica addition on flowability, strength and transport properties of ultra high performance concrete, Mater. Des. 59 (2014) 1–9.
[55] E. Ghafari, S.A. Ghahari, Y. Feng, F. Severgnini, N. Lu, Effect of Zinc oxide and Al-Zinc oxide nanoparticles on the rheological properties of cement paste, Composites B 105 (2016) 160–166.
[56] Y. Xu, D.D.L. Chung, Cement of high specific heat and high thermal conductivity, obtained by using silane and silica fume as admixtures, Cem. Concr. Res. 30 (7) (2000) 1175–1178.
[57] R. Demirboğa, Thermal conductivity and compressive strength of concrete incorporation with mineral admixtures, Build. Environ. 42 (7) (2007) 2467–2471.
[58] R. Demirboğa, Influence of mineral admixtures on thermal conductivity and compressive strength of mortar, Energy Build. 35 (2) (2003) 189–192.

[59] R. Demirboğa, Rüstem Gül, The effects of expanded perlite aggregate, silica fume and fly ash on the thermal conductivity of lightweight concrete, Cem. Concr. Res. 33 (5) (2003) 723–727.
[60] F. Blanco, P. Garcıa, P. Mateos, J. Ayala, Characteristics and properties of lightweight concrete manufactured with cenospheres, Cem. Concr. Res. 30 (11) (2000) 1715–1722.
[61] A. Loudon, The thermal properties of lightweight concretes, Int. J. Cem. Compos. Lightweight Concr. 1 (2) (1979) 71–85.
[62] X. Fu, D.D.L. Chung, Effect of admixtures on thermal and thermomechanical behavior of cement paste, ACI Mater. J. 96 (4) (1999).